18. An estimated albedo is derived by dividing *I/F* (determined from observations calibrated with the onboard calibration target) by the cosine of the solar elevation angle at the time of each observation. This albedo estimate should be comparable to the bolometric Lambert albedo values derived from orbital observations.
19. B. Hapke, *Theory of Reflectance and Emittance Spectroscopy* (Cambridge Univ. Press, New York, 1993).
20. J. R. Johnson *et al.*, *J. Geophys. Res.* **104**, 8809 (1999).
21. R. Greeley *et al.*, *Lunar Planet. Sci. Conf. XXXV*, abstr. 2162 (Lunar and Planetary Institute, Houston, TX, 2004) [CD].
22. R. V. Morris *et al.*, *Geochim. Cosmochim. Acta* **57**, 4597 (1993).
23. R. V. Morris *et al.*, *J. Geophys. Res.* **105**, 1757 (2000).
24. J. L. Bishop *et al.*, *J. Geophys. Res.* **103**, 31457 (1998).
25. R. V. Morris *et al.*, in *Mineral Spectroscopy: A Tribute to Roger G. Burns*, M. D. Dyar, C. McCammon, M. W. Schaefer, Eds. (Geochemical Society, Houston, TX, 1996), pp. 327–336.
26. R. V. Morris *et al.*, *J. Geophys. Res.* **100**, 5319 (1995).
27. R. V. Morris, D. C. Golden, *Icarus* **134**, 1 (1998).
28. P. R. Christensen *et al.*, *Science* **306**, 1733 (2004).
29. Both pyroxene and olivine exhibit broad Fe^{2+} absorption bands centered near 900 to 1100 nm [e.g., (*30*, *31*)], but because the long-wavelength sides of these bands are typically beyond the spectral range of silicon CCD detectors, it is usually not possible to uniquely identify the specific Fe^{2+}-bearing phases responsible for reflectance decreases observed in the longest wavelength filters of instruments such as Pancam (*32*).
30. J. B. Adams, *J. Geophys. Res.* **79**, 4829 (1974).
31. E. A. Cloutis *et al.*, *J. Geophys. Res.* **91**, 11641 (1986).
32. E. A. Cloutis, J. F. Bell III, *Icarus* **172**, 233 (2004).
33. M. T. Lemmon *et al.*, *Science* **306**, 1753 (2004).
34. J. F. Bell III *et al.*, in preparation.
35. We extend our sincere gratitude to the many hundreds of people who have contributed to the success of the Pancam investigation. These include the many MER engineers, managers, and support staffers at JPL; engineers and researchers at many vendor organizations; students and support staff at Cornell University, USGS/Flagstaff, Washington University, and other institutions; image processing and visualization experts at JPL and NASA/Ames Research Center; and many of the co-investigators, collaborators, and associates on the Athena Science Team. We also extend special thanks to our families and loved ones for their patience and support during mission operations and throughout the many years leading up to our spectacular travels on Mars.

Plates Referenced in Article
www.sciencemag.org/cgi/content/full/306/5702/1703/DC1
Plates 1, 2, 4 to 7, and 9 to 16

15 September 2004; accepted 15 October 2004

RESEARCH ARTICLE

In Situ Evidence for an Ancient Aqueous Environment at Meridiani Planum, Mars

S. W. Squyres,[1]* J. P. Grotzinger,[2] R. E. Arvidson,[3] J. F. Bell III,[1] W. Calvin,[4] P. R. Christensen,[5] B. C. Clark,[6] J. A. Crisp,[7] W. H. Farrand,[8] K. E. Herkenhoff,[9] J. R. Johnson,[9] G. Klingelhöfer,[10] A. H. Knoll,[11] S. M. McLennan,[12] H. Y. McSween Jr.,[13] R. V. Morris,[14] J. W. Rice Jr.,[5] R. Rieder,[15] L. A. Soderblom[9]

Sedimentary rocks at Eagle crater in Meridiani Planum are composed of fine-grained siliciclastic materials derived from weathering of basaltic rocks, sulfate minerals (including magnesium sulfate and jarosite) that constitute several tens of percent of the rock by weight, and hematite. Cross-stratification observed in rock outcrops indicates eolian and aqueous transport. Diagenetic features include hematite-rich concretions and crystal-mold vugs. We interpret the rocks to be a mixture of chemical and siliciclastic sediments with a complex diagenetic history. The environmental conditions that they record include episodic inundation by shallow surface water, evaporation, and desiccation. The geologic record at Meridiani Planum suggests that conditions were suitable for biological activity for a period of time in martian history.

The primary objective of the Mars Exploration Rover mission is to search for evidence in the martian geologic record of environmental conditions that might once have been suitable for life. Elsewhere in this issue (*1*) we describe the geologic setting in and around Eagle crater (*2*), the small impact crater in Meridiani Planum where the rover Opportunity landed. Here, we describe rocks exposed in the wall of Eagle crater in more detail and consider their implications for past aqueous processes and habitability.

Stratigraphy and sedimentology. The outcrop at Eagle crater can be mapped (Fig. 1) on the basis of color, morphology, texture, and structural attitude revealed in Pancam images (*3*). The maximum stratigraphic thickness exposed at any location within the outcrop is about 30 to 50 cm. Although the units we have mapped reveal a complex stratigraphy, intense brecciation associated with the impact event hinders reconstruction of the relative ages. Postdepositional surface weathering and collapse may also have contributed to brecciation.

The western part of the outcrop forms map unit A and includes an area called Shoemaker's Patio up to the point marked by the Slickrock fault. This unit is characterized by large breccia blocks and by the highest albedo (~0.30) within the outcrop when viewed in bulk. Bedding within blocks shows dips of 0° to 15°, defined by fine planar lamination, low-angle cross-stratification, and cross-bed sets as thick as 7 cm (Fig. 2A). Embedded spherules are present, but vugs are rare to absent. The margins of some breccia blocks show rims with raised relief and redder colors (*3*).

Map unit B, extending from the Slickrock fault northeastward toward the rock called El Capitan, is characterized by large blocks that are lower in albedo than those in map unit A. Bedding within the blocks is steep on the east side of the fault, with dips up to 60° as observed at Slickrock and a rock called the Dells. Bedding within unit B is characterized by planar lamination to low-angle cross-stratification (Fig. 2B), ripple cross-lamination (Plate 7), and crinkly to undulatory lamination (Fig. 2C). Embedded spherules and vugs are abundant.

Map unit C includes El Capitan and other rocks along the northern and outer margin of Eagle crater. Bedding planes are nearly horizontal, and bedding is more poorly expressed than elsewhere. In the upper part of El Capitan (Guadalupe), the bedding is only faintly visible. Embedded spherules are present and vugs are abundant. The upper part of

[1]Department of Astronomy, Cornell University, Ithaca, NY 14853, USA. [2]Department of Earth, Atmospheric, and Planetary Sciences, Massachusetts Institute of Technology, Cambridge, MA 02139, USA. [3]Department of Earth and Planetary Sciences, Washington University, St. Louis, MO 63031, USA. [4]Department of Geological Sciences, University of Nevada, Reno, NV 89557, USA. [5]Department of Geological Sciences, Arizona State University, Tempe, AZ 85287, USA. [6]Lockheed Martin Corporation, Littleton, CO 80127, USA. [7]Jet Propulsion Laboratory, California Institute of Technology, Pasadena, CA 91109, USA. [8]Space Science Institute, Boulder, CO 80301, USA. [9]U.S. Geological Survey, Flagstaff, AZ 86001, USA. [10]Johannes Gutenberg University, D-55128 Mainz, Germany. [11]Botanical Museum, Harvard University, Cambridge, MA 02138, USA. [12]Department of Geosciences, State University of New York, Stony Brook, NY 11794, USA. [13]Department of Earth and Planetary Sciences, University of Tennessee, Knoxville, TN 37996, USA. [14]NASA Johnson Space Center, Houston, TX 77058, USA. [15]Max-Planck-Institut für Chemie, Kosmochemie, D-55128 Mainz, Germany.

*To whom correspondence should be addressed. E-mail: squyres@astrosun.tn.cornell.edu

unit C has greater relief than the lower part, a more massive appearance, a redder and more mottled color, and possibly a greater amount of intergranular cement. It is also the strongest material found in Eagle crater, as revealed by Rock Abrasion Tool (RAT) grinding energy (*4*).

Map unit D includes the eastern part of the outcrop, named Big Bend. This unit is characterized by relatively intact stratigraphy, with dips of 20° to 30° that define a northeast-plunging open fold. The outcrop here exhibits strong eolian etching parallel to bedding, giving it a ribbed appearance. Sedimentary structures include ripple cross-lamination (Plate 6) and crinkly bedding. Spherules are present, but vugs are rare to absent.

Map unit E represents zones within the outcrop consisting of brecciated blocks with or without visible bedding, but for which no other attributes can be assigned, in some areas because the rover did not examine them in sufficient detail.

Microscale texture. Microscopic Imager (MI) images (*5*) reveal four physical constituents in the outcrop. The primary component consists of moderately rounded medium to coarse sand-sized grains; these grains are well sorted within laminae but show some variations in grain size among layers. Especially in the well-laminated rocks of unit B, individual laminations are a single grain thick, with lamina thickness varying from 0.3 mm to nearly 1 mm (Fig. 2D). The second component is the gray spherules that are embedded in all units of the outcrop (Fig. 3). Spherule diameters are typically 4 to 6 mm. The third component is cement, which is fine-grained through much of the unit. Locally, coarser millimeter-scale cement crystals are observed to form sockets around some spherules (*5*). Finally, vugs are common in some units (Fig. 4). The vugs have tabular prismatic shapes and random orientations that cut across lamination, and they intersect the surface to form openings with typical widths of 1 to 2 mm and lengths of ~1 cm. Sharp angles are common for vugs not rounded by weathering; in particular, many vugs are thickest in the middle and taper toward both ends.

Chemistry and mineralogy. The elemental composition of the Eagle crater outcrop, as measured with the Alpha Particle–X-Ray Spectrometer (APXS), is most noteworthy for high concentrations of sulfur, with nearly 25 weight percent SO_3 found in some locations (*6*). This proportion of S is greater than that in typical Meridiani soils (*7*) by a factor of ~5 and greater than in the basaltic rocks at the Gusev crater landing site investigated by Spirit (*8*) by a factor of nearly 20. Although S is strongly enriched in the Eagle crater outcrop, Cl is not; hence, if both are present in salts, fractionation by differential solubility may have occurred.

Overall, the high concentrations of S in the outcrop are most readily explained by high abundances of sulfate salts. Mineralogic observations from the Mössbauer spectrometer and the Miniature Thermal Emission Spectrometer (Mini-TES) confirm this interpretation. The Mössbauer spectrometer has detected the ferric sulfate mineral jarosite $[(K,Na,H_3O,X^{+1})Fe_3(SO_4)_2(OH)_6]$ in all exposures of the outcrop (*9*), and Mini-TES spectra of the outcrop indicate ~20 to 40% by weight of Mg and Ca sulfates (*10*).

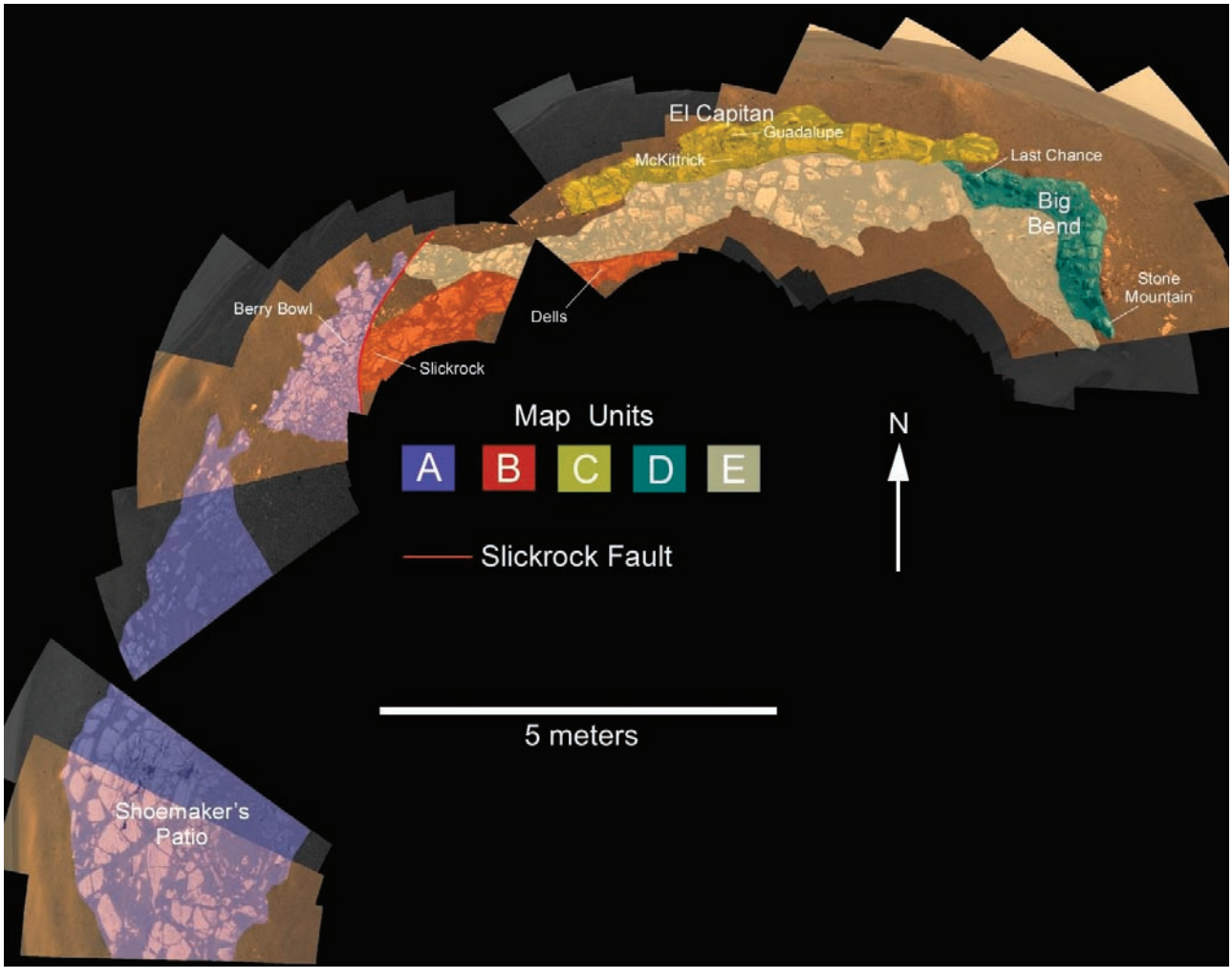

Fig. 1. Pancam images of the outcrop in Eagle crater, in a vertical projection overlain with map units.

Another noteworthy characteristic of the outcrop rocks is that the concentration of bromine is highly variable, ranging from 30 ppm or less to as much as 440 ppm (*6*). These variations are found over small length scales; Br concentrations in two RAT holes in El Capitan (Guadalupe and McKittrick) differ by more than an order of magnitude, even though their locations differ by only 20 cm in elevation. The lowest Br concentrations in the outcrop yield Cl/Br ratios comparable to the chondritic Cl/Br ratio, whereas the highest are substantially enhanced in Br. Bromides are generally more soluble than chlorides of the same cations, and large local enhancements in Br relative to Cl are sometimes found in terrestrial evaporite deposits (*11*, *12*).

On Earth, the most common +1 cation in jarosite is K^+, but K is impoverished in the outcrop and Na^+ or H_3O^+ must compensate. The most abundant available cation by far is Mg^{2+}. One or more hydrated Mg sulfate salts, such as kieserite, hexahydrite, and/or epsomite, may be present. Adequate Na is available for halite, although bischofite [$MgCl_2 \cdot 6(H_2O)$] or antarcticite [$CaCl_2 \cdot 6(H_2O)$] could be present. Ca sulfates (anhydrite, bassanite, gypsum) may also be found in the outcrop, as well as various double salts with Na^+, such as bloedite, vanthoffite, or glauberite. These geochemical inferences are supported by the Mini-TES data that indicate substantial quantities of Mg and Ca sulfates. If all the Mg and two-thirds of the Ca are in the form of sulfates, the balance of the S can be accounted for by jarosite. Most of these candidate salts, including the jarosite detected by the Mössbauer spectrometer, are hydrated compounds, probably providing at least some of the hydrogen atoms that have been detected from orbit over Meridiani Planum by the Mars Odyssey Gamma-Ray Spectrometer experiment (*13*).

Along with sulfate salts, the outcrop rock must contain a substantial fraction of siliciclastic materials. APXS data show that the elemental composition of this component is basaltic in character (*6*), but evidence for primary igneous minerals is weak. Mini-TES detections of small amounts of olivine, pyroxene, and feldspar in outcrop exposures are best explained as surface contamination by the abundant wind-blown basaltic sand (*10*). The Mössbauer spectrometer detected no olivine in outcrop rock exposed by the RAT, and only a weak feature that is provisionally

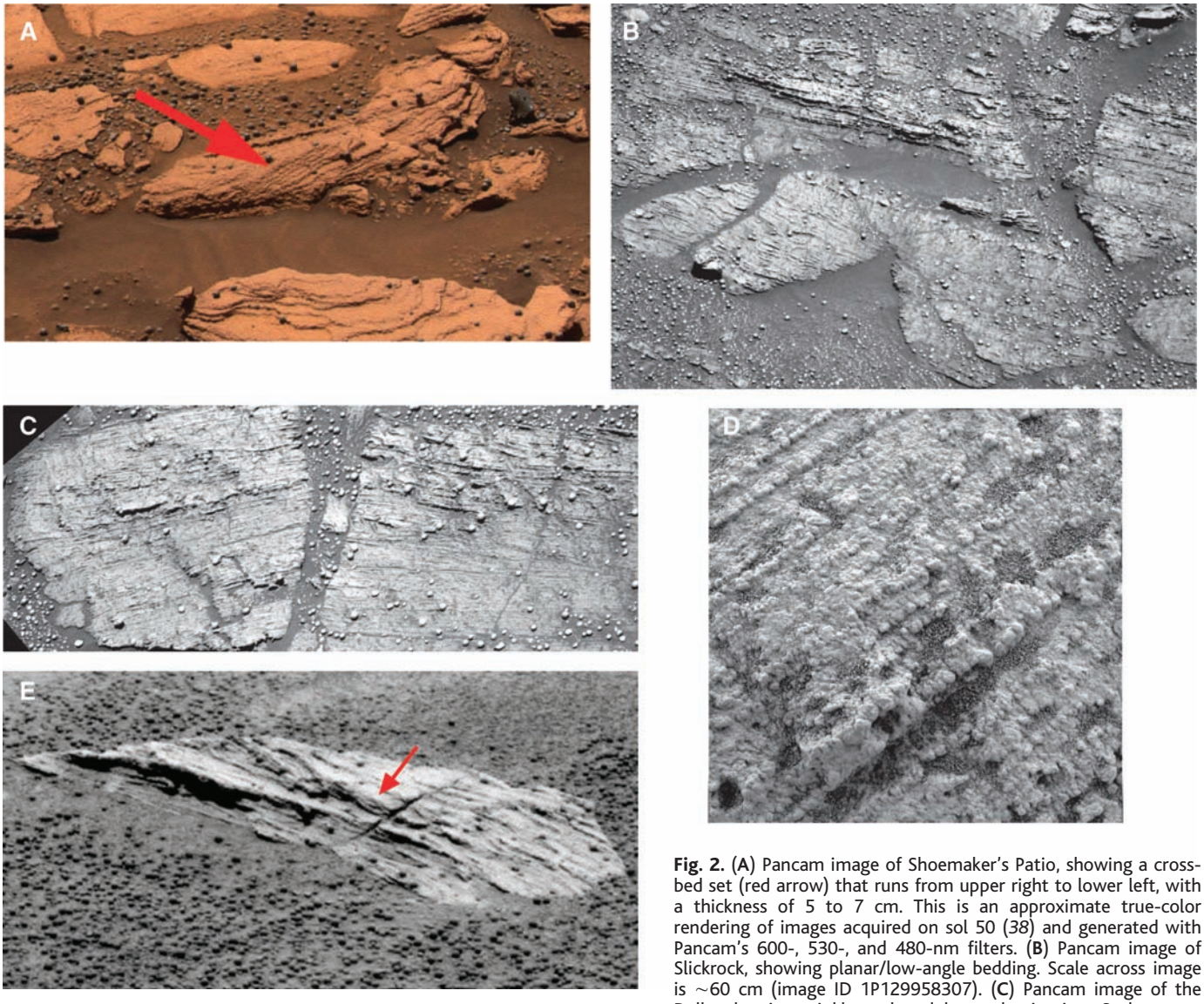

Fig. 2. (**A**) Pancam image of Shoemaker's Patio, showing a cross-bed set (red arrow) that runs from upper right to lower left, with a thickness of 5 to 7 cm. This is an approximate true-color rendering of images acquired on sol 50 (*38*) and generated with Pancam's 600-, 530-, and 480-nm filters. (**B**) Pancam image of Slickrock, showing planar/low-angle bedding. Scale across image is ~60 cm (image ID 1P129958307). (**C**) Pancam image of the Dells, showing crinkly and undulatory lamination. Scale across image is ~55 cm (image ID 1P131822391). (**D**) MI image of laminations that are a single grain thick. Scale across image is ~30 mm (image ID 1M131912465). (**E**) Pancam image of Scoop, a rock just outside Eagle crater, showing small-scale ripple cross-lamination with festoon geometry (red arrow). Scale across image is ~40 cm. Sum of six left-eye images obtained on sol 52.

assigned to pyroxene but that could be some other Fe^{2+} phase (*9*).

The spherules differ in composition from the rock in which they are embedded. Pancam images show that the spherules have distinctly different visible and near-infrared spectral properties than the rock (*3*). Because the spherules are much smaller than the fields of view of the APXS and Mössbauer instruments, it is not possible to isolate individual spherules for detailed compositional analysis by these instruments. However, two independent observations demonstrate that their composition is dominated by hematite. First, Mini-TES observations of spherules that lie atop Meridiani soil show that the concentration of hematite as detected by Mini-TES correlates with the fraction of the Mini-TES field of view filled by spherules (*10*). Second, a Mössbauer measurement was made on an accumulation of loose spherules that are fortuitously concentrated together in a local topographic depression in the outcrop named the Berry Bowl. This measurement shows a strong hematite signal relative to a measurement made on spherule-free outcrop immediately adjacent to the Berry Bowl (*9*).

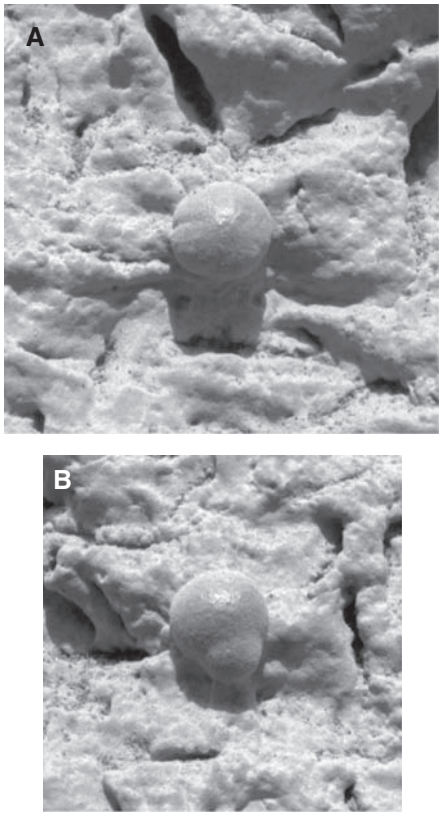

Fig. 3. (**A**) MI image of a spherule showing banding across it, aligned with local lamination in the surrounding sediments. Scale across image is ~15 mm (image ID 1M130760791). (**B**) A "doublet" spherule formed by two interpenetrating spherules. Scale across image is ~13 mm (image ID 1M130672582).

Other observations also point to a strong hematite concentration in the spherules. APXS measurements of the Berry Bowl show anomalously high Fe and a high Fe/Mn ratio (*6*). Pancam spectra of spherules are also indicative of hematite (*3*), and spherules sectioned with the RAT show consistent Pancam spectral properties throughout their interiors, indicating that the hematite is not simply present in coatings. Indeed, the spherules, which are strewn across most soils at the Opportunity landing site (*14*), both inside Eagle crater and on the surrounding plains, appear to be the primary carriers of the coarse-grained gray hematite that was detected from orbit by the Mars Global Surveyor TES instrument (*15*). Not all hematite is in spherules, however, because the Mössbauer spectrometer also detects hematite in spherule-free outcrops (*6*), albeit at lower concentrations than in the spherules. Grinding of the outcrop with the RAT consistently produces a pronounced brick-red stain in the RAT cuttings (*3*). This color differs from that of the outcrop and is consistent with production of fine-grained hematite, perhaps from both the rock and the spherules, during the grinding process.

Cross-stratification. Stratification styles observed in the rocks of Eagle crater include planar lamination, low-angle cross-stratification, cross-bedding, ripple cross-lamination, and crinkly and undulatory lamination.

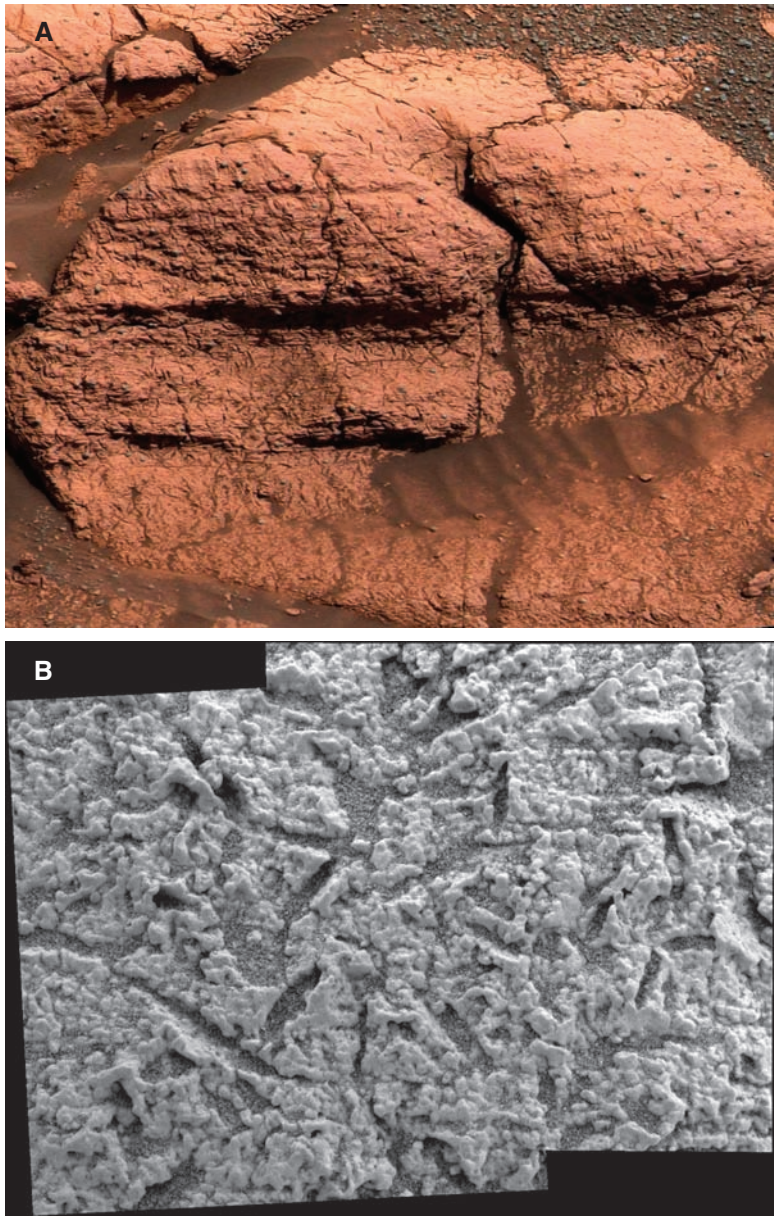

Fig. 4. (**A**) Pancam image of vugs in El Capitan, acquired on sol 27 and generated with Pancam's 750-, 530-, and 480-nm filters. Scale across image is ~43 cm (image ID 1M130670922). (**B**) MI mosaic of vugs in El Capitan. Scale across each individual image frame is 30 mm (image IDs 1M130670922 and 1M130671284).

Planar lamination and low-angle cross-stratification are well developed in several locations, particularly at Slickrock and Shoemaker's Patio. MI images at Slickrock show laminations of single-grain thick layers (Fig. 2D) suggestive of eolian sediment transport (*16*). At Shoemaker's Patio, a single cross-bed set with thickness of 5 to 7 cm is preserved (Fig. 2A). The set is truncated at either end because of brecciation, so bed set geometry is unconstrained, but cross-strata lap downward tangentially against the lower bounding surface. This geometry represents deposition of either subaerial or subaqueous dunes (*17*). The presence of adjacent breccia blocks with planar lamination and low-angle cross-lamination suggests that eolian processes may have been dominant here, perhaps forming in response to the passage of adhesion ripples on an aggrading and moist depositional surface.

In contrast, ripple cross-lamination with festoon geometry is present at the rock called Last Chance (Big Bend area; Plate 6), at the Dells (Plate 7), and in an isolated rock called Scoop (Fig. 2E) on the southwest rim of the crater. Ripple cross-laminae sets are 0.8 to 1.7 cm thick. The sets at Scoop may be climbing. These geometries indicate sediment transport in subaqueous ripples. The reconstructed former bedforms are inferred to be only a few centimeters in size and are therefore too small to be eolian dunes (*17*, *18*). But they are also too large (and of the wrong geometry) to be the climbing translatent cross-strata produced by eolian wind ripples (*16*, *19*). Their size is, however, consistent with subaqueous formation. Also, their festoon geometry requires that the reconstructed ripples have three-dimensional geometry defined by highly sinuous crestlines. Such bedforms are known only to develop in subaqueous, subcritical flows, with velocities as fast as a few tens of centimeters per second (*17*, *18*, *20*). Mars' lower gravity has only a small effect on the initiation of sediment transport and bedform size (*20*, *21*), posing no challenge to the subaqueous interpretation.

Diagenetic features. The rocks exposed in Eagle crater exhibit a complex diagenetic history. Observed diagenetic features are consistent with formation within the fluid-saturated (phreatic) zone of a groundwater system (*22*, *23*). There is minimal disruption of primary sedimentary features, which suggests that diagenetic processes involved little bulk volume change.

The most conspicuous diagenetic features are the hematitic spherules (Fig. 3). These are found in all rock exposures in Eagle crater and represent ~2% of the rock by volume. They exhibit a narrow size range, and their shapes deviate only slightly from spherical. Spherules sectioned by the RAT lack internal structure at scales visible to the MI (*5*). The spatial distribution of spherules within outcrop rock is more uniform than a spatially random (i.e., Poisson) distribution; in particular, they are not concentrated along bedding planes. Spherules generally do not disturb surrounding laminations, but some show banding or grooves that parallel the lamination in the rock that immediately surrounds them (Fig. 3A). Most spherules occur as single bodies, but occasionally they are found as doublets or triplets (Fig. 3B). Their resistance to weathering and to grinding with the RAT (*4*) indicates that spherules are harder than the surrounding rock.

On the basis of these characteristics and their hematite-dominated composition, we interpret the spherules as concretions that formed during early burial diagenesis, after the primary phase of compaction and under near-isotropic permeability and near-static fluid conditions (*24*, *25*). Their formation may have involved replacement of preexisting sulfate minerals and filling of primary porosity. The fact that the concretions formed within sandy sediments but do not preserve sandy textures in their interiors suggests that dissolution was involved and that the siliciclastic grains within the rock are much smaller than sand size. The exact chemical reactions involved in spherule formation are not well constrained, but breakdown of jarosite to form hematite during a period of fluid recharge is thermodynamically plausible.

The vugs (Fig. 4) are unevenly distributed at Eagle crater, but in the rocks where they are present, they typically cover about 5% of the surface. When abraded by the RAT (providing a deeper view into the rock), the apparent size of vugs can expand; this suggests that they are related to chemical dissolution rather than physical erosion. Because of this characteristic, and especially because of their tabular shape, we interpret the vugs to represent a crystal-mold porosity (*26*) formed by dissolution of a relatively soluble mineral phase (or phases), likely sulfates.

Crosscutting relationships suggest that the concretions postdated the formation of the primary vug-filling minerals, and that the development of secondary porosity that yielded the vugs postdated the formation of concretions (Fig. 5). Because spherules crosscut and truncate vugs, the vug-filling minerals presumably were present first. But there is no perturbation of the spherical shape of concretions where vugs abut against them or where concretions impinge into vug space; this finding implies that the secondary porosity was not present when the concretions formed.

In addition to spherule and vug formation, one or more episodes of cementation may have taken place in the outcrop rock. Lithification is likely related to pore-filling cement consisting of sulfate minerals and possibly hematite. Parts of the outcrop (e.g., Guadalupe) are much more resistant to the RAT and have a more massive appearance where freshly exposed, perhaps because of a locally higher degree of cementation and/or an episode of recrystallization. In places, exposed concretions are surrounded by a socket that could represent another generation of recrystallization.

History. We interpret the rocks of the Eagle crater outcrop to be a mixture of chemical and siliciclastic sediments with a complex diagenetic history. The environmental conditions that they record are episodic inundation by surface water to shallow depths, followed by evaporation, exposure, and desiccation. The festoon cross-lamination provides evidence for inundation by water, the mineralogy and geochemistry indicate precipitation of dissolved salts, and the planar to low-angle lamination and larger scale cross-bedding are consistent with sediment transport across a dry surface. Terrestrial analogs for such a suite of facies and surface processes include interdune depressions

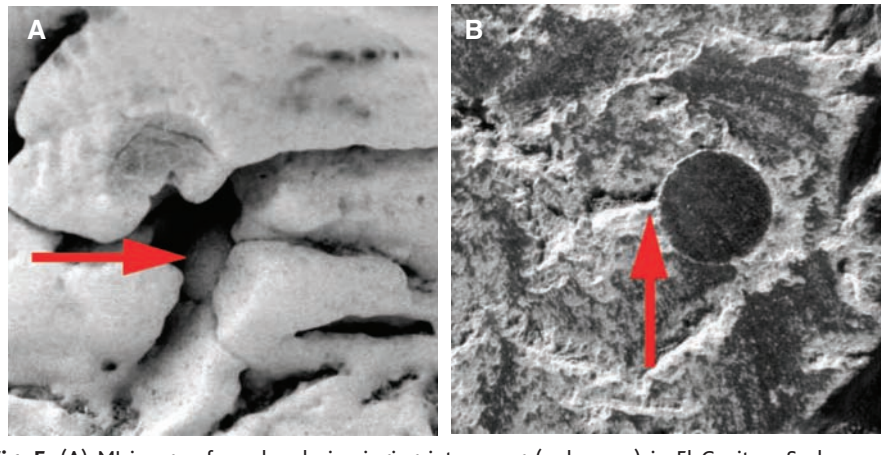

Fig. 5. (**A**) MI image of a spherule impinging into a vug (red arrow) in El Capitan. Scale across image is ~12 mm (image ID 1M130762242). (**B**) MI image of a spherule crosscutting a vug (red arrow) in a portion of El Capitan that was exposed by the RAT. Scale across image is ~12 mm (image ID 1M131212783).

(*27*), playa lakes (*28*), and sabkhas adjacent to marginal seaways (*29*).

Our elemental and mineralogic data suggest that the sedimentary rocks are, by weight, ~50% fine-grained siliciclastic materials derived from basaltic rocks, ~40% sulfate minerals (including Mg sulfate and jarosite), and ~10% hematite. Primary igneous minerals are not readily identified in the siliciclastic fraction, suggesting a substantial degree of chemical alteration. The sulfate minerals may have formed via direct precipitation from water or within the sediment during early burial. In the intervals when surface water was present, it may have been open to the martian atmosphere, but in the absence of unambiguous wave ripples we cannot rule out the possibility of an ice cover.

Aqueous and eolian transport of sulfate-rich sand grains was followed by cementation by fine-grained material, probably mostly sulfates and perhaps also hematite. Concretions formed via precipitation of hematite from groundwater, and tabular mineral grains (probably sulfates) grew. Subsequent diagenetic events included local recrystallization of cements and dissolution of the soluble mineral grains to form vugs. All of these processes were followed after an unknown time interval by the formation of Eagle crater itself, exposing the sedimentary rocks and causing much of the observed brecciation.

It is noteworthy that the environmental conditions recorded at Eagle crater may have prevailed over a large area. All of the bedrock observed during Opportunity's traverse to Endurance crater, more than half a kilometer from the landing site, showed the same characteristics as the outcrop in Eagle crater (*1*). More important, orbital data from the Mars Orbiter Camera show that a relatively high-albedo unit that correlates with the outcrop exposures near the Opportunity landing site is at least discontinuously present across most of Meridiani Planum. It seems likely, then, that the area over which these aqueous sedimentary and diagenetic processes operated was at least tens of thousands of square kilometers in size.

The timing and duration of aqueous processes at Meridiani are more difficult to determine. The crater size frequency distributions for the Meridiani plains suggest a complex history of crater production and removal (*30*), compromising our ability to extract useful ages from crater abundances. An upper bound on the age can be derived from analyses of orbital images showing that the Meridiani plains materials disconformably overlie dissected Middle to Late Noachian cratered terrains (*31*), which suggests that the rocks in Eagle crater could be as much as several billion years old. Nothing in our observations at Eagle crater places useful bounds on the duration of aqueous activity at Meridiani.

Implications. Liquid water, which our results show was once abundant at Meridiani Planum, is widely viewed as a key prerequisite for life. Therefore, we infer that surface conditions at Meridiani may have been habitable for some period of time in martian history.

The recorded environmental conditions, however, would have posed at least two kinds of challenges to development of martian biology. One set of challenges deals with water chemistry. Mineral assemblages similar to those in Eagle crater are found on Earth. Commonly these are associated with mine drainage, but in some cases, notably the Rio Tinto basin in Spain (*32*), mineral deposition predates mining activity. Precipitating waters tend to be acidic, sometimes strongly so. In addition, in the saline waters suggested by Meridiani geology, water activity could have been at least episodically prohibitive.

High acidity and salinity do not pose insurmountable challenges to microbial life on Earth. Acidic waters can support a phylogenetically wide array of bacteria and microscopic eukaryotes (*33*, *34*); microorganisms can also accommodate to both short-term desiccation and (within limits) persistent hypersalinity (*35*). Such organisms, however, belong to specialized populations that have evolved to survive in highly acidic or saline environments. It is less clear that such conditions are suitable for the kinds of prebiotic chemical reactions commonly invoked to explain the origin of life.

A second class of challenges to biology at Meridiani deals with the persistence of water. The rocks at Eagle crater expose tens of centimeters of sulfate-rich stratigraphy. At nearby Endurance crater, the exposed thickness of similar rocks approaches 10 m. Despite this substantial thickness, the apparent prevalence of sulfate-cemented eolian sands suggest that water on Meridiani Planum may have been regionally extensive but temporally discontinuous, increasing the difficulty of biological persistence over long time intervals.

We cannot determine whether life was present or even possible in the waters at Meridiani, but it is clear that by the time the sedimentary rocks in Eagle crater were deposited, Mars and Earth had already gone down different environmental paths. Sample return of Meridiani rocks might well provide more certainty regarding whether life developed on Mars. Sulfate deposits are known to preserve both chemical and morphological fossils (*36*), and iron oxide precipitates at Rio Tinto contain beautifully preserved fossils, including minute fossils of coccoid and filamentous microorganisms (*37*). Meridiani Planum therefore can be considered an attractive candidate for further study, both by landed missions and by sample return.

References and Notes

1. S. W. Squyres *et al.*, *Science* **306**, 1698 (2004).
2. Names have been assigned to aerographic features by the Mars Exploration Rover (MER) team for planning and operations purposes. The names are not formally recognized by the International Astronomical Union.
3. J. F. Bell III *et al.*, *Science* **306**, 1703 (2004).
4. R. E. Arvidson *et al.*, *Science* **306**, 1730 (2004).
5. K. E. Herkenhoff *et al.*, *Science* **306**, 1727 (2004).
6. R. Rieder *et al.*, *Science* **306**, 1746 (2004).
7. The term martian soil is used here to denote any loose unconsolidated materials that can be distinguished from rocks, bedrock, or strongly cohesive sediments. No implication of the presence or absence of organic materials or living matter is intended.
8. R. Gellert *et al.*, *Science* **305**, 829 (2004).
9. G. Klingelhöfer *et al.*, *Science* **306**, 1740 (2004).
10. P. R. Christensen *et al.*, *Science* **306**, 1733 (2004).
11. L. A. Hardie, *Am. J. Sci.* **284**, 193 (1984).
12. L. A. Hardie, *Annu. Rev. Earth Planet. Sci.* **19**, 131 (1991).
13. W. V. Boynton *et al.*, *Science* **297**, 81 (2002).
14. L. A. Soderblom *et al.*, *Science* **306**, 1723 (2004).
15. P. R. Christensen *et al.*, *J. Geophys. Res.* **105**, 9623 (2000).
16. R. E. Hunter, D. M. Rubin, in *Eolian Sediments and Processes*, M. E. Brookfield, T. S. Ahlbrandt, Eds. (Elsevier, Amsterdam, 1983), pp. 429–454.
17. J. C. Harms *et al.*, *Structures and Sequences in Clastic Rocks* (Society of Economic Paleontologists and Mineralogists, Tulsa, OK, 1982).
18. G. V. Middleton, J. B. Southard, *Mechanics of Sediment Movement* (Society of Economic Paleontologists and Mineralogists, Providence, RI, 1984).
19. D. M. Rubin, R. E. Hunter, *Sedimentology* **29**, 121 (1982).
20. J. B. Southard, J. A. Boguchwal, *J. Sediment. Petrol.* **66**, 680 (1990).
21. P. L. Wiberg, J. D. Smith, *Water Resour. Res.* **23**, 1471 (1987).
22. L. A. Hardie *et al.*, in *Sixth Symposium on Salt* (Northern Ohio Geological Society, Cleveland, 1983), pp. 11–39.
23. J. P. Smoot, T. K. Lowenstein, in *Evaporites, Petroleum, and Mineral Resources*, J. L. Melvin, Ed. (Elsevier, Amsterdam, 1991), pp. 189–347.
24. J. Sellés-Martínez, *Earth Sci. Rev.* **41**, 177 (1996).
25. A. Seilacher, *Sediment. Geol.* **143**, 41 (2001).
26. P. W. Choquette, L. C. Pray, *Am. Assoc. Petrol. Geol. Bull.* **54**, 207 (1970).
27. N. P. Mountney, D. B. Thompson, *Sedimentology* **49**, 805 (2002).
28. R. W. Renault, W. M. Last, *Sedimentology and Geochemistry of Modern and Ancient Saline Lakes* (Society of Economic Paleontologists and Mineralogists, Tulsa, OK, 1994).
29. D. J. Kinsman, *Am. Assoc. Petrol. Geol. Bull.* **53**, 830 (1969).
30. M. D. Lane *et al.*, *Geophys. Res. Lett.* **30**, 10.1029/2003GLO17183 (2003).
31. R. E. Arvidson *et al.*, *J. Geophys. Res.* **108**, 10.1029/2002JE002041 (2003).
32. D. C. Fernández-Remolar, N. Rodriguez, F. Gómez, R. Amils, *J. Geophys. Res.* **108**, 10.1029/2002JE001918 (2003).
33. L. Ameral Zettler *et al.*, *Nature* **417**, 137 (2002).
34. B. J. Baker, J. F. Banfield, *FEMS Microbiol. Ecol.* **44**, 139 (2003).
35. D. Billi, M. Potts, *Res. Microbiol.* **153**, 7 (2002).
36. S. Bonny, B. Jones, *Can. J. Earth Sci.* **40**, 1483 (2003).
37. D. Fernández-Remolar, R. Amils, R. V. Morris, A. H. Knoll, *Proceedings of the 33rd Lunar and Planetary Science Conference* (Houston, TX, March 2002), abstr. 1226.
38. A martian solar day has a mean period of 24 hours 39 min 35.244 s and is referred to as a sol to distinguish this from a roughly 3% shorter solar day on Earth.
39. This research was carried out for the Jet Propulsion Laboratory, California Institute of Technology, under a contract with NASA.

Plates Referenced in Article

www.sciencemag.org/cgi/content/full/306/5702/1709/DC1
Plates 6 and 7

26 August 2004; accepted 19 October 2004